Talanta 82 (2010) 196–201

Contents lists available at ScienceDirect

Talanta

journal homepage: www.elsevier.com/locate/talanta

Direct electrocatalytic oxidation of nitric oxide and reduction of hydrogen peroxide based on α-Fe_2O_3 nanoparticles-chitosan composite

Li Zhang, Yonghong Ni*, Xinghong Wang, Guangchao Zhao

College of Chemistry and Materials Science, Anhui Key Laboratory of Functional Molecular Solids, Anhui Normal University, Beijing East Road No. 1, Wuhu 241000, PR China

ARTICLE INFO

Article history:
Received 11 January 2010
Received in revised form 9 April 2010
Accepted 9 April 2010
Available online 24 April 2010

Keywords:
α-Fe_2O_3 nanoparticles
Chitosan
Nitric oxide
Hydrogen peroxide
Non-enzymatic amperometric sensor

ABSTRACT

α-Fe_2O_3 nanoparticles prepared using a simple solution-combusting method have been dispersed in chitosan (CH) solution to fabricate nanocomposite film on glass carbon electrode (GCE). The as-prepared α-Fe_2O_3 nanoparticles were characterized by powder X-ray diffraction (XRD), scanning electron microscopy (SEM). The nanocomposite film exhibits high electrocatalytic oxidation for nitric oxide (NO) and reduction for hydrogen peroxide (H_2O_2). The electrocatalytic oxidation peak is observed at +0.82 V (vs. Ag/AgCl) and controlled by diffusion process. The electrocatalytic reduction peak is observed at −0.45 V (vs. Ag/AgCl) and controlled by diffusion process. This α-Fe_2O_3–CH/GCE nanocomposite bioelectrode has response time of 5 s, linearity as 5.0×10^{-7} to 15.0×10^{-6} M of NO with a detection limit of 8.0×10^{-8} M and a sensitivity of −283.6 μA/mM. This α-Fe_2O_3–CH/GCE nanocomposite bioelectrode was further utilized in detection of H_2O_2 with a detection limit of 4.0×10^{-7} M, linearity as 1.0×10^{-6} to 44.0×10^{-6} M and with a sensitivity of 21.62 μA/mM. The shelf life of this bioelectrode is about 6 weeks under room temperature conditions.

1. Introduction

Nitric oxide (NO) has been shown to be an important bioregulator molecule involved in physiological functions such as blood pressure control, neurotransmission, and immune surveillance [1]. In order to clarify the function and to control the concentration in biological systems, selective and sensitive detection of NO is of great importance. However, the detection and quantification of NO is particularly difficult because of its low concentration, short half-time, low stability [2], and high reactivity with superoxide and other very active free radicals present in biological systems [3]. Among a variety of techniques for probing NO, electrochemical techniques are reported especially well suited for the development of analytical approaches for NO because of their inherent sensitivity and possibility of giving results in real time. Monitoring of NO with electrochemical sensors has been achieved at multiwalled carbon nanotubes modified electrodes [4,5], manganese porphyrin/polypyrrole films [6], nickel porphyrinato complexes [7], vitamin B_{12} film [8], and TiO_2–Au nanocomposite film electrodes [9], as well as proteins such as cytochrome c [10], hemoglobin and myoglobin [11,12] immobilized at electrode surfaces. Although some chemically modified electrodes have been proposed to reduce the large overpotential required for the direct oxidation of NO [4–10], it is interesting to develop new materials with high efficiency and small dimensions for the detection of NO.

Like NO, H_2O_2 is another often studied analyte in various fields including clinic, food, pharmaceutical and environmental analyses because H_2O_2 is a chemical threat to the environment and the production of enzymatic reactions [13]. Many methods have been developed for the determination of H_2O_2, such as spectrophotometry [14], chromatography [15] and chemiluminescence [16]. Compared with the above detection methods, however, the electrochemical detection of H_2O_2 attracts wider interest owing to its low detection limit and low cost. Electrochemical sensors, such as amperometric biosensors, have been appeared as the most convenient tools for hydrogen peroxide determination; especially enzyme modified electrode has been usually used [17–19]. However, native enzymes gradually lose their catalytic activity after repeated measurements. Therefore, a development of novel electrocatalyst which overcomes the disadvantages of native enzymes is desired. In recent years, with the development of nanotechnology, many ways have been tried to circumvent this problem. Many kinds of nanoscale materials, such as ordered mesoporous carbon [20], Ag microspheres [21], CuO nanoparticles [22], Mn–nitrilotriacetate acid nanowires [23], and MnO_2 nanoparticles [24,25] have been used in the construction of biosensors because of their unique and particular properties.

The emergence of nanotechnology is opening new horizons for electrochemical sensors [26,27]. Nanoparticles, nanotubes, nanowires such as Au [28], CuS [29], Fe_2O_3 [30], MWNTs [31] and Si [32] have been extensively used in the field of electro-

* Corresponding author. Tel.: +86 553 3869303; fax: +86 553 3869303.
E-mail address: nyh314@mail.ahnu.edu.cn (Y. Ni).

0039-9140/$ – see front matter © 2010 Elsevier B.V. All rights reserved.
doi:10.1016/j.talanta.2010.04.018

chemical biosensors due to their small size, large surface area, high surface reaction activity, high catalytic efficiency and corresponding potential electronic and chemical properties [22]. Among these nanomaterials, magnetic nanoparticles have recently gained increased interest due to promising applications as drug delivery and biosensors, etc. [33,34]. Hematite (α-Fe_2O_3), as an environment-friendly n-type semiconductor (E_g = 2.1 eV) and the most thermodynamically stable phase of iron oxide under ambient conditions, is drawing intense interest not only for its unique properties but also for its applications in many fields such as catalysis, gas sensors, magnetic recording media, lithium-ion batteries, anticorrosive agents, water treatment, and pigments [35–38]. Chitosan along with nanoparticles has been utilized as a stabilizing agent due to its biocompatibility, film-forming ability, nontoxicity, and high mechanical strength [39]. Herein, we report the preparation of α-Fe_2O_3 nanoparticles via a simple solution-combusting method and their applications to the electrochemical biosensing of NO and H_2O_2 by embedding α-Fe_2O_3 nanoparticles in chitosan matrix.

2. Experimental

2.1. Reagents and apparatus

Chitosan was obtained from Hefei BoMei Biotechnology Company. Saturated NO solutions were prepared as the previous literature [40]. In detail, the double-distilled water was bubbled with high purity nitrogen for 30 min to remove oxygen and then the water was bubbled with pure NO gas for 30 min to prepare a NO saturated solution. The water used in all experiments was double distilled with a quartz apparatus. NO standards were prepared by making serial dilutions of saturation NO solutions with deoxygenated phosphate buffer solutions (pH 7.0) [41]. We first prepared NO saturation, and then extracted the required volume of NO solution with an injector. After that, we infused the above NO solution in the injector into the basic electrolyte. High purity nitrogen gas was used for de-aeration. 30% H_2O_2 solution was purchased from Beijing Chemical Reagent Factory (Beijing, China). All chemicals used were analytical grade. Double-distilled water was used for preparation of buffer and standard solutions. H_2O_2 solution was diluted daily before the electrochemical measurements.

Electrochemical experiments were performed with CHI 440a electrochemical analyzer (ChenHua Instruments Co., Ltd., Shanghai, China) with a conventional three-electrode cell. The α-Fe_2O_3–CH/GCE, an Ag/AgCl and a platinum electrode was used as the working electrode, the reference and the auxiliary electrode, respectively.

2.2. Synthesis of α-Fe_2O_3 nanoparticles

The synthesis of α-Fe_2O_3 nanoparticles has been reported in our previous work [42]. In a typical synthesis, $FeCl_3{\cdot}6H_2O$ of 0.02 mol was dissolved in 100 ml mixed solvents of ethanol and ethyleneglycol with the volume ratio of 60/40. After the solution was transferred into a spirit lamp with an absorbent cotton lampwick, the spirit lamp was fired. For a moment, some red substance was produced on the top of the lampwick. When the lampwick was extinguished, the red product was collected, repeatedly washed with distilled water to remove the impurities. Finally, the product was dried at 50 °C in air for 5 h.

2.3. Characterization of the samples

Powder X-ray diffraction (XRD) of the product was carried out on a Shimadzu XRD-6000 X-ray diffractometer equipped with Cu Kα radiation (λ = 0.154060 nm), employing a scanning rate of 0.02 s^{-1} and 2θ ranges from 15° to 80°. Field emission scanning electron microscopy (SEM) was obtained by JEOL JSM-6700 FESEM (operating at 10 kV).

2.4. Electrode modification

The dispersed α-Fe_2O_3 nanoparticles on the electrode were fabricated by the following way: firstly, the glass carbon electrode (GCE, Φ = 3 mm) was polished with a 1700# diamond paper and washed successively with double-distilled water and ethanol in an ultrasonic bath, then 15 cyclic scans were carried out in the potential of 2.0 to −2.0 V (vs. SCE) in the solution of 1.0 mol/l H_2SO_4. Secondly, a CH solution was prepared by dissolving CH (25 mg) in 50 ml of acetate buffer (0.05 M, pH 4.2) solution. The optimized ratio of CH and Fe_2O_3 nanoparticles was 5:1 by stirring at room temperature after it was sonicated to prepare α-Fe_2O_3–CH nanocomposite film. Then 15 μl solution of α-Fe_2O_3–CH composite was cast onto a glass carbon electrode and dried in air. Thus, an α-Fe_2O_3–CH modified GCE was obtained.

2.5. Electrochemical analysis of nitric oxide and hydrogen peroxide

For optimizing the determination conditions of NO and H_2O_2, a number of buffer systems were tested, including 0.1 mol/l HAc–NaAc (pH 5.6), 0.1 mol/l NaH_2PO_4–NaOH (pH 7.0), 0.1 mol/l KCl. In general, the similar results were presented, but somewhat higher sensitivity was obtained in the phosphate buffer. Hence, measurements were carried out in NaH_2PO_4–NaOH buffers. Another reason we chose the phosphate buffer as the supporting electrolyte is that it is closer to the natural environments of NO in organisms as well as H_2O_2 in real samples.

The effect of the applied potential on the response current of the α-Fe_2O_3–CH nanocomposite modified electrode was also studied. The maximum response current was observed at +0.82 V for NO and −0.45 V for H_2O_2. Thus a potential +0.82 V and −0.45 V was selected as the optimum applied potential, respectively.

3. Results and discussion

3.1. Structures and morphology characterization

Fig. 1a shows the XRD pattern of the as-prepared product. All diffractions can be indexed as the hexagonal-phase α-Fe_2O_3 by comparison with JCPDS card files No. 86-0550 (a = 5.035 Å and c = 13.74 Å). No characteristic peaks of other iron oxides such as Fe_3O_4 and γ-Fe_2O_3 are detected. The strong and narrow diffraction peaks reveal that the product has high crystallinity and rather big particle size. A typical SEM image is shown in Fig. 1b, from which the average size of nanoparticles is measured to be ∼100 nm.

3.2. Electrochemical property of α-Fe_2O_3–CH composite modified GCE

Fig. 2 shows the cyclic voltammetric responses of various electrodes in an oxygen-free 0.1 M phosphate buffer solution (PBS, pH 7.0). No redox peak was observed when the CH/GCE was used as the work electrode (Fig. 2a). While the α-Fe_2O_3–CH/GCE was employed as the work electrode, a pair of well-defined redox peaks was obtained (Fig. 2b) with an average formal potential of −0.088 V. The cathodic peak and anodic peak were −0.141 and −0.035 V at a scan rate of 0.05 V/s, respectively. This agrees well with the previous report on the direct electron transfer of nanostructured Fe_2O_3 onto tin-doped indium oxide (ITO) [43,44] and nanotube Fe_2O_3 onto Au disk electrode [30]. The redox peaks can be ascribed to the redox reaction of α-Fe_2O_3 nanoparticles entrapped in the chitosan composite film.

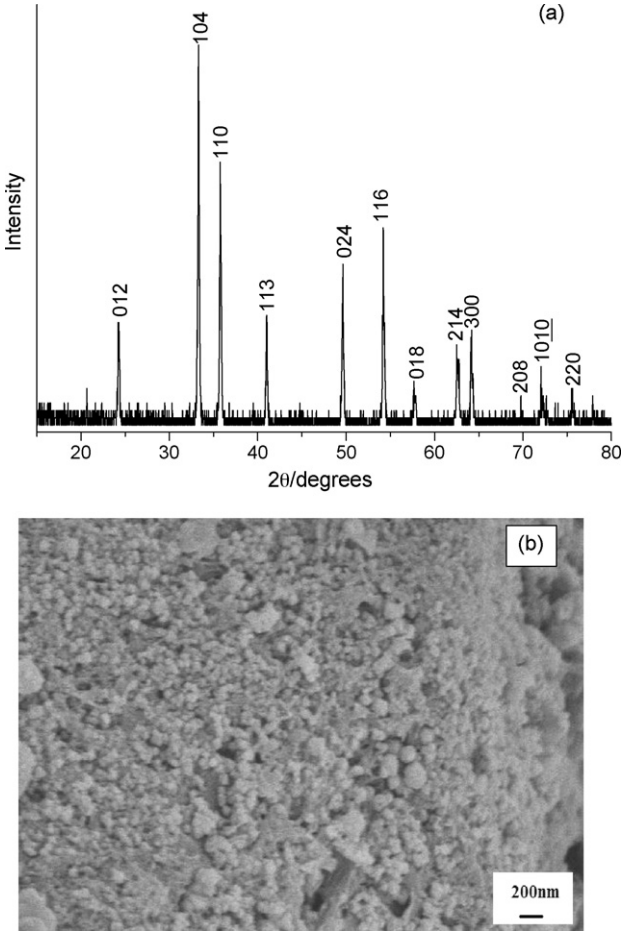

Fig. 1. (a) The XRD pattern and (b) SEM image of the product.

Fig. 3 depicts the cyclic voltammograms of the α-Fe_2O_3–CH/GCE in 0.1 M PBS (pH 7.0) at different scan rates. As can be seen, both cathodic and anodic peak currents increased linearly with the scan rate (ν) from 0.02 to 0.2 V/s. This result reveals the electron transfer of α-Fe_2O_3–CH complex with the GCE in an adsorption electrochemical process.

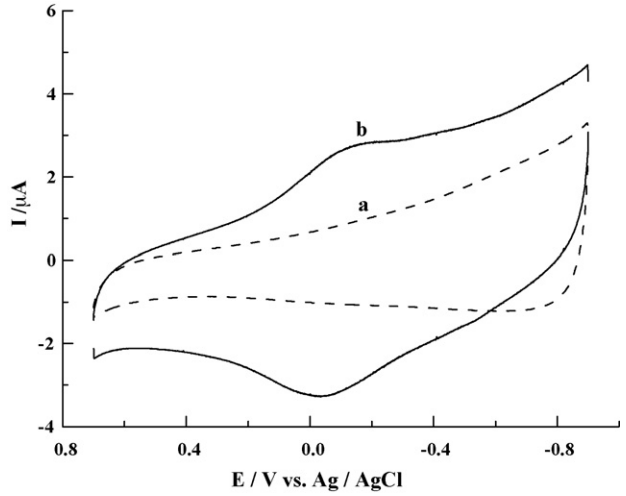

Fig. 2. Cyclic voltammograms recorded in an oxygen-free 0.1 M PBS (pH 7.0) at the scan rate of 0.05 V/s, using various modified electrodes: (a) CH/GCE and (b) α-Fe_2O_3–CH/GCE.

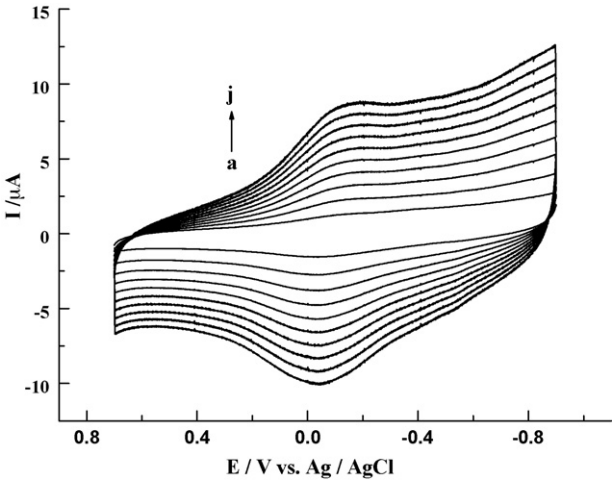

Fig. 3. Cyclic voltammograms of the α-Fe_2O_3–CH/GCE in deoxygenized 0.1 M PBS (pH 7.0) at different scan rates (from inside to outside: a → j: 0.02, 0.04, 0.06, 0.08, 0.10, 0.12, 0.14, 0.16, 0.18, 0.20 V/s, respectively).

3.3. Electrooxidation behavior and amperometric response of NO on the α-Fe_2O_3–CH/GCE

Fig. 4 shows typical CVs of the α-Fe_2O_3–CH/GCE in the absence and presence of NO, at the scan rate of 0.05 V/s in the oxygen-free 0.1 M PBS (pH 7.0). With the addition of NO into solution, an obvious anodic peak was observed at 0.82 V and the peak current increased significantly with NO concentration increased (see b–e in Fig. 4). In phosphate buffer solution containing 100 μM NO, the cyclic voltammograms of NO at the α-Fe_2O_3–CH/GCE and CH/GCE were shown in the inset of Fig. 4. At the CH/GCE, the CV of NO demonstrated a wave with anodic peak potential (E_{pa}) at 0.928 V. While at the α-Fe_2O_3–CH/GCE, the anodic peak potential shifted negatively to 0.821 V and the peak current (i_{pa}) increased significantly, which implied that α-Fe_2O_3 nanoparticles entrapped in the composite film greatly facilitated the oxidation of NO. α-Fe_2O_3 nanoparticles distributed in chitosan matrix provide abundant active sites for functional sensing of NO, and thus dramatically facilitate oxidation of NO.

Regarding the oxidation peak of NO at α-Fe_2O_3–CH/GCE, the potential scan rate was investigated clearly as shown in Fig. 5. The peak current is proportional to the square root of scan rate

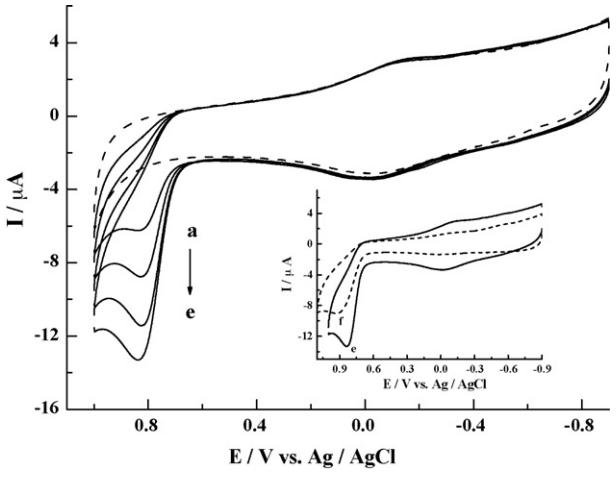

Fig. 4. Cyclic voltammograms of NO in 0.1 M PBS of pH 7.0 for α-Fe_2O_3–CH/GCE in various concentrations: (a) 0 μM, (b) 25 μM, (c) 50 μM, (d) 75 μM, and (e) 100 μM at scan rate of 50 mV s^{-1}. Inset: CVs of 100 μM NO at CH/GCE (f) and α-Fe_2O_3–CH/GCE (e) in the same condition.

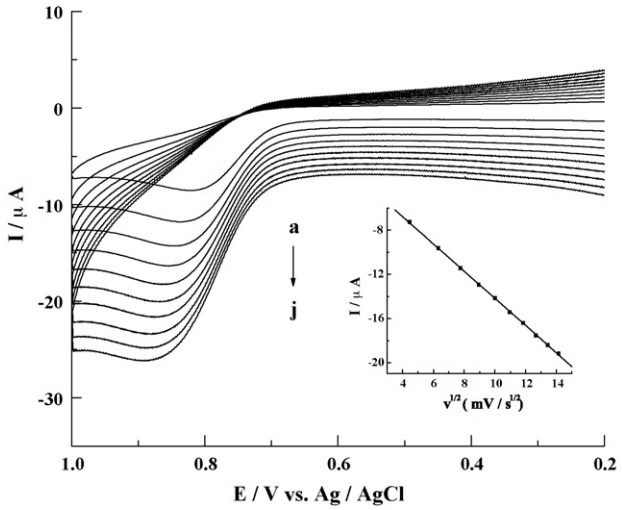

Fig. 5. CVs of 100 μM NO at the α-Fe_2O_3-CH/GCE in deoxygenized 0.1 M PBS (pH 7.0) at different scan rates (from inside to outside: a → j: 0.02, 0.04, 0.06, 0.08, 0.10, 0.12, 0.14, 0.16, 0.18, 0.20 V/s, respectively). The linear dependence of peak current with the square root of scan rate was shown in the inset.

in the range of 20–200 mV s^{-1}, $i_{pa}/\mu A = -1.839 - 1.233\nu^{1/2}/mV\,s^{-1}$, $R = 0.9992$, while the E_{pa} shifted positively. The results suggested that the oxidation of NO was undergoing a diffusion controlled process.

The mechanism of NO oxidation can be assumed as following: NO is adsorbed by the hybrid material firstly and then the removal of electrons from NO to the hybrid material does occur. The results are from the collective role of the chitosan (CH) and α-Fe_2O_3 nanoparticles, because it has been shown that the oxidation of NO occurs at CH, but its detection is less sensitive than at CH-α-Fe_2O_3. This highly sensitive determination can be explained by the CH-α-Fe_2O_3 structure. Having the sponge-like porous structure, CH can provide a base for the mediation for NO at CH-α-Fe_2O_3 modified electrode with Fe_2O_3 as a mediator. In that case, the oxidative Fe (III) and the reductive Fe (II) on Fe_2O_3 are reduced and oxidized, respectively [20].

Fig. 6 illustrates current–time plots for the α-Fe_2O_3–CH/GCE under the optimized experimental conditions with successive step changes of NO concentration. As the NO was injected into the

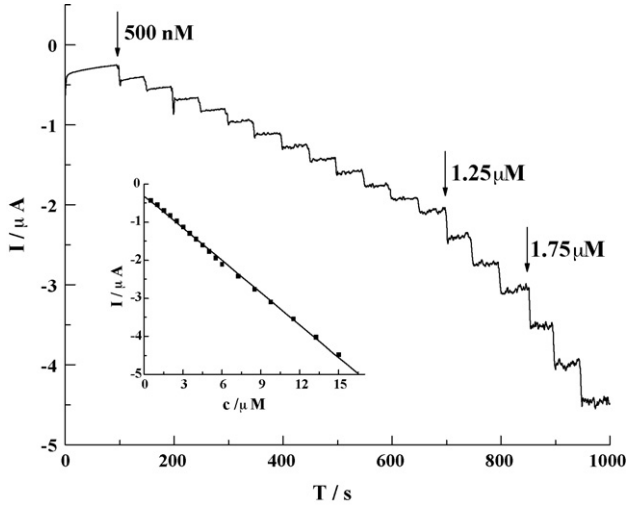

Fig. 6. Amperometric responses of α-Fe_2O_3–CH/GCE upon the successive addition of NO into gently stirred 0.1 M PBS at 0.82 V. Inset: the linear relationships between the catalytic current and the concentration.

Table 1
Comparison of performance of various NO sensors.

Electrode materials	Applied potential (V)	Detection limit (μM)	Reference
MWNTs/GCE/Nf	0.72	0.08	[4]
MWNTs–ACB film	0.75	0.028	[5]
Mn (II)TCPPyP	0.72	0.1	[6]
Cyt c/L-cysteine/Au	0.824	0.3	[10]
α-Fe_2O_3–CH/GCE	0.82	0.08	This work

stirring PBS, the steady-state currents reached another steady-state value (95% of the maximum) in less than 5 s. Such a fast response implies that the α-Fe_2O_3 can promote the oxidation of NO. The linear relationship between the catalytic current and the concentration is shown in the inset of Fig. 6. As can be seen, the α-Fe_2O_3–CH/GCE displays linear response range of 5.0×10^{-7} to 15.0×10^{-6} M (correlation coefficient: 0.9972), with a detection limit of 8.0×10^{-8} M at a signal-to-noise ratio of 3 and a sensitivity of −283.6 μA/mM. We have summarized various NO sensors in Table 1 with respect to the operating conditions and the detection limit. It can be seen that the performance of the developed sensor is comparable to most of NO sensors in literature in one or more categories.

3.4. Electroreduction behavior and amperometric response of H_2O_2 on the α-Fe_2O_3–CH/GCE

Fig. 7 shows the cyclic voltammograms of the α-Fe_2O_3–CH/GCE in the absence and presence of H_2O_2. When H_2O_2 was added to the pH 7.0 PBS, compared with the system with no H_2O_2 present (a), an obvious increase of the reduction peak was observed in deoxygenized environment (b–d). However, no electrochemical reduction peak was observed when the cyclic voltammetric scan was performed at CH/GCE under the same conditions (inset in Fig. 5). The experimental results indicated that the α-Fe_2O_3–CH/GCE exhibited excellent electrocatalytic activity to H_2O_2.

Regarding the reduction peaks of H_2O_2 at α-Fe_2O_3–CH/GCE, the effect of potential scan rate was investigated clearly. As shown in Fig. 8, the reduction peak current is proportional to the square root of scan rate in the range of 10–100 mV s^{-1}, $i_{pa}/\mu A = 0.659 + 0.408\nu^{1/2}/mV\,s^{-1}$, $R = 0.9987$, indicating a diffusion controlled process.

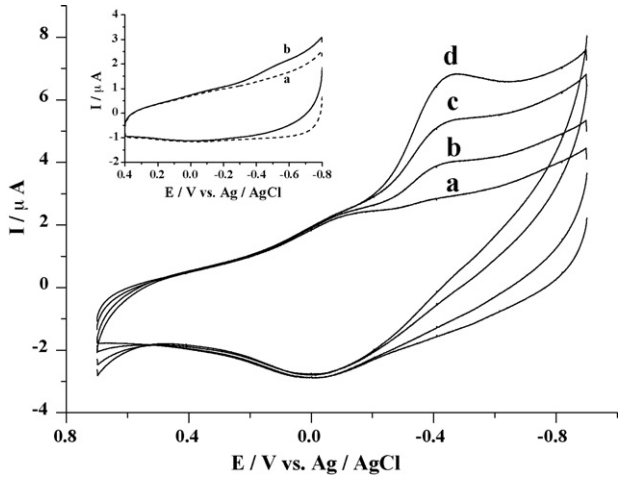

Fig. 7. Cyclic voltammograms of H_2O_2 in 0.1 M PBS of pH 7.0 for α-Fe_2O_3–CH/GCE in various concentrations: (a) 0 mM, (b) 0.05 mM, (c) 0.2 mM, and (d) 0.4 mM at scan rate of 50 mV s^{-1}. Inset: CVs of H_2O_2 at CH/GCE in various concentrations: (a) 0 mM and (b) 0.4 mM.

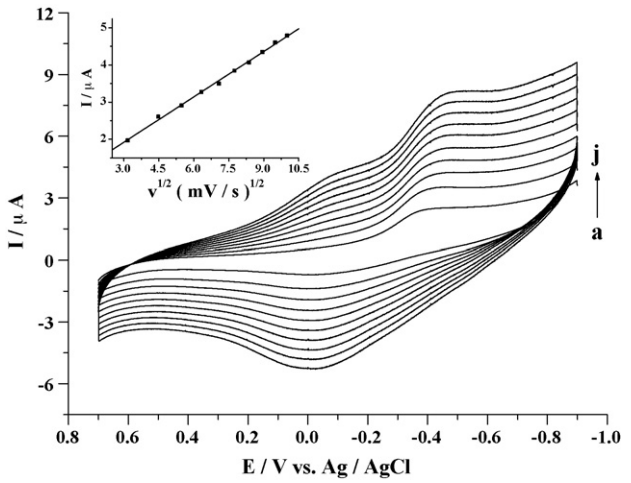

Fig. 8. CVs of 0.2 mM H_2O_2 at the α-Fe_2O_3–CH/GCE in deoxygenized 0.1 M PBS (pH 7.0) at different scan rates (from inside to outside: a → j: 0.01, 0.02, 0.03, 0.04, 0.05, 0.06, 0.07, 0.08, 0.09, 0.10 V/s, respectively). The linear dependence of peak current with the square root of scan rate was shown in the inset.

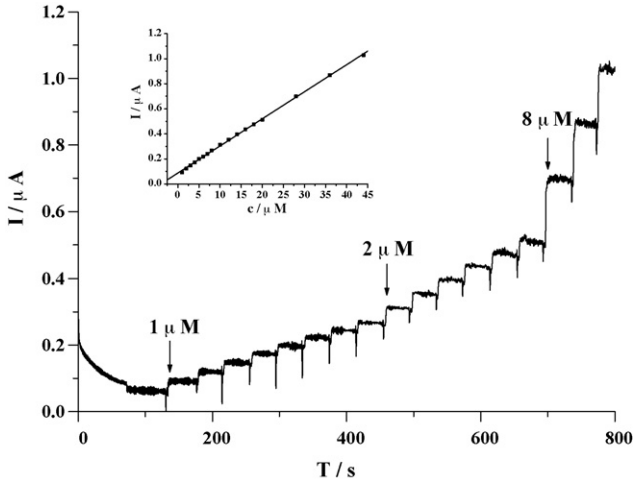

Fig. 9. Amperometric responses of α-Fe_2O_3–CH/GCE upon the successive addition of H_2O_2 into gently stirred 0.1 M PBS at −0.45V. Inset: the linear relationships between the catalytic current and the concentration.

The catalytic mechanism for the reduction of H_2O_2 can be assumed as following: Fe (III) was first electrochemically reduced to Fe (II) on the hybrid material CH-α-Fe_2O_3, and then Fe (II) reacted with H_2O_2, which resulted in the conversion of H_2O_2 to H_2O and in the regeneration of the catalyst [19,22]. We also investigated the electrode modified by α-Fe_2O_3 without CH, which showed that α-Fe_2O_3 tended to peel off from the electrode surface. Thus CH in the hybrid film provides a stable and high performance supporting platform for α-Fe_2O_3.

Fig. 9 illustrates current–time plots for the α-Fe_2O_3–CH/GCE under the optimized experimental conditions with successive step changes of H_2O_2 concentration. As the H_2O_2 was injected into the stirring PBS, the steady-state currents reached another steady-state value (95% of the maximum) in less than 5s. Such a fast response implies that the α-Fe_2O_3 can promote the oxidation of H_2O_2. The linear relationship between the catalytic current and the concentration is shown in the inset of Fig. 9. As can be seen, the α-Fe_2O_3–CH/GCE displays linear response range of 1.0×10^{-6} to 44.0×10^{-6} M (correlation coefficient: 0.9997), with a detection limit of 4.0×10^{-7} M at a signal-to-noise ratio of 3 and a sensitivity of 21.62 μA/mM. We have summarized various H_2O_2 sensors in Table 2 with respect to the operating conditions, sensitivity, and the detection limit. Compared with other reported values [19–23] in Table 2, α-Fe_2O_3–CH/GCE exhibits the comparable detection limit and the highest sensitivity.

3.5. Accuracy, selectively and stability of the α-Fe_2O_3–CH/GCE

The accuracy was evaluated by successive determinations of 2.0×10^{-6} M NO and 4.0×10^{-6} H_2O_2 for 6 times using the same electrode, respectively. The relative standard deviation (R.S.D.) was calculated to be 2.7% and 4.8%, indicating the applicability and acceptable accuracy of our built sensors.

Some chemical species were tested to check their levels of interference in the NO determination. The results showed that most of the ions, such as K^+, Na^+, Ag^+, Mg^{2+}, Zn^{2+}, Ni^{2+}, Cl^-, SO_4^{2-} and PO_4^{3-}, 50-fold amount of these ions had little effect on the determination. The compounds that could react with NO, such as oxygen, etc., disturbed the determination of NO because they decreased the concentration of NO in solution. NH_3 was found little effect on the determination of NO. The possible interfering species on current response of H_2O_2 was also examined. Glucose, cysteine and NH_3 induced no effect on the steady-state current to H_2O_2. The steady-state current to H_2O_2 was reduced to 92% of original response by subsequent addition of ascorbic acid. Therefore, the α-Fe_2O_3–CH/GCE possesses high selectively. The stability of the electrode was also tested. When the electrode was stored at room temperature for 1 week, the CV peak currents still retained 97.3% and 96.5% for NO and H_2O_2, respectively. In the next 5 weeks the response still retained 88% and 84.3% of the initial value, respectively.

3.6. Real sample analysis

As an example of a real sample, the concentration of H_2O_2 in the medical disinfectant (3%) was determined using the biosensor. The real concentration of the store solution was firstly detected by the potassium permanganate titration method, which was employed as the reference method. The samples containing desirable concentrations of H_2O_2 were then prepared by diluting suitable amount of medical disinfectant samples with 0.1 M PBS (pH 7.0). The mean concentrations of H_2O_2 in samples were detected to be 2.42×10^{-6} and 16.70×10^{-6} M, with the R.S.D.% of 7.3% and 2.1%, respectively. Compared with the real concentrations of 2.69×10^{-6} and 16.84×10^{-6} M, the results were in acceptable agreement and good reproducibility. Thus, the proposed method could be used as in the detection limit range.

Table 2
Comparison of performance of various H_2O_2 sensors.

Electrode materials	Applied potential (V)	Detection limit (μM)	Sensitivity (μA/mM)	Reference
Nafion/Mb/CGNs/GCE	−0.45	0.5	–	[19]
Ordered mesoporous carbon	−0.2	0.036	8.4	[20]
Ag microspheres/Nafion	−0.5	1.2	–	[21]
CuO nanoparticles	−0.3	0.06	–	[22]
Mn–NTA nanowires/Nafion	0.7	0.2	5.58	[23]
α-Fe_2O_3–CH/GCE	−0.45	0.4	21.62	This work

The concentration of NO added to 0.1 M PBS (pH 7.0) containing possible interference of foreign matter was also determined using the biosensor. When 800 nM NO was added to 0.1 M PBS (pH 7.0), the average recovery of the biosensor was 94.3% ($n = 4$). The possible interference of foreign matter, which might occur in real samples, was investigated. When the concentrations of K^+, Pb^{2+}, Cd^{2+}, Zn^{2+}, Ni^{2+}, NH_3, Cl^-, $SO_4{}^{2-}$ and $PO_4{}^{3-}$ in the sample were 50 times that of NO, no significant interference was observed. However in the presence of the same concentration of oxygen, the peak current showed a decrease of approximately 10%. These results proved that the sensor has potential applications in determination of NO real samples.

4. Conclusions

Polycrystalline α-Fe_2O_3 nanoparticles have been successfully prepared by a simple solution-combusting method without any requirement of calcinations step at high temperature. A natural polymer, chitosan, has been used as a dispersant of α-Fe_2O_3. The nanocomposite film is very stable on the surface of glass carbon electrode and exhibits high electrocatalytic oxidation for nitric oxide and electrocatalytic reduction of hydrogen peroxide. Its sensitivity, repeatability and stability are satisfactory. Furthermore, this synthetic approach can also be applied for the synthesis of other inorganic oxides with improved performances and they can also be extended to construct other nanostructured functional surfaces.

Acknowledgements

The authors thank the National Natural Science Foundation of China (20771005 and 20571002), Science and Technological Fund of Anhui Province for Outstanding Youth (08040106834), Young Fund of Anhui Normal University (2008xqn61) for fund support.

References

[1] S. Moncada, R.M.J. Palmer, Pharmacol. Rev. 43 (1991) 109–142.
[2] S.H. Snyder, D.S. Bredt, Sci. Am. 266 (1992) 68–71.
[3] M. Kelm, M. Feelish, R. Spahr, H.M. Piper, E. Noak, J. Schurader, Biochem. Biophys. Res. Commun. 154 (1988) 236–244.
[4] F.H. Wu, G.C. Zhao, X.W. Wei, Electrochem. Commun. 4 (2002) 690–694.
[5] D. Zheng, C. Hu, Y. Peng, W. Yue, S. Hu, Electrochem. Commun. 10 (2008) 90–94.
[6] N. Diab, W. Schuhmann, Electrochim. Acta 47 (2001) 265–273.
[7] S. Trevin, F. Bedioui, J. Devynck, J. Electroanal. Chem. 408 (1996) 261–265.
[8] S.L. Vilakazi, T. Nyokong, Electrochim. Acta 46 (2000) 453–461.
[9] E.V. Milsom, J. Novak, M. Oyama, Frank Marken, Electrochem. Commun. 9 (2007) 436–442.
[10] Y.C. Liu, S.Q. Cui, J. Zhao, Z.S. Yang, Bioelectrochemistry 70 (2007) 416–420.
[11] J.T. Pang, C.H. Fan, X.J. Liu, T. Chen, G.X. Li, Biosens. Bioelectron. 19 (2003) 441–445.
[12] G.C. Zhao, L. Zhang, X.W. Wei, Z.S. Yang, Electrochem. Commun. 5 (2003) 825–829.
[13] S. Yao, J. Xu, Y. Wang, X. Chen, Y. Xu, S. Hu, Anal. Chim. Acta 557 (2006) 78.
[14] A. Lobnik, M. Cajlakovic, Sens. Actuators B: Chem. 74 (2001) 194–199.
[15] U. Pinkernell, S. Effkemann, U. Karst, Anal. Chem. 69 (1997) 3623–3627.
[16] F.R.P. Rocha, E.R. Torralba, B.F. Reis, A.M. Rubio, M. de la Guardia, Talanta 67 (2005) 673–677.
[17] A.K. Upadhyay, T.W. Ting, S.M. Chen, Talanta 79 (2009) 38–45.
[18] H.Y. Zhao, W. Zheng, Z.X. Meng, H.M. Zhou, X.X. Xu, Z. Li, Y.F. Zheng, Biosens. Bioelectron. 24 (2009) 2352–2357.
[19] W. Yang, Y. Li, Y. Bai, C. Sun, Sensors Actuators B 115 (2006) 42–48.
[20] J.C. Ndamanisha, Y. Hou, J. Bai, L. Guo, Electrochim. Acta 54 (2009) 3935–3942.
[21] B. Zhao, Z. Liu, Z. Liu, G. Liu, Z. Li, J. Wang, X. Dong, Electrochem. Commun. 11 (2009) 1707–1710.
[22] X.M. Miao, R. Yuan, Y.Q. Chai, Y.T. Shi, Y.Y. Yuan, J. Electroanal. Chem. 612 (2008) 157–163.
[23] S. Liu, L. Li, Q. Hao, X. Yin, M. Zhang, Q. Li, L. Chen, T. Wang, Talanta 81 (2010) 727–731.
[24] X. Zheng, Z. Guo, Talanta 50 (2000) 1157–1162.
[25] Y. Lin, X. Cui, L. Li, Electrochem. Commun. 7 (2005) 166–172.
[26] J. Wang, Analyst 130 (2005) 421–426.
[27] J. Wang, A.S. Arribas, Small 2 (2006) 129–134.
[28] H.Y. Gu, A.M. Yu, H.Y. Chen, J. Electroanal. Chem. 516 (2001) 119–126.
[29] X. Zhang, G. Wang, A. Gu, Y. Wei, B. Fang, Chem. Commun. (2008) 5945–5947.
[30] J. Gong, L. Wang, K. Zhao, D. Song, Electrochem. Commun. 10 (2008) 123–126.
[31] H.T. Zhao, H.X. Ju, Anal. Biochem. 350 (2006) 138–144.
[32] M.W. Shao, Y.Y. Shan, N.B. Wong, S.T. Lee, Adv. Func. Mater. 15 (2005) 1478–1482.
[33] F.Y. Cheng, C.H. Su, Y.S. Yang, C.S. Yeh, C.Y. Tsai, C.L. Wu, M.T. Wu, D.B. Shie, Biomaterials 26 (2005) 729–738.
[34] L.M. Rossi, A.D. Quach, Z. Rosenzweig, Anal. Bioanal. Chem. 380 (2004) 606–613.
[35] S.H. Zhan, D.R. Chen, X.L. Jiao, S.S. Liu, J. Colloids Interface Sci. 308 (2007) 265–270.
[36] J. Chen, L. Xu, W. Li, X. Gou, Adv. Mater. 17 (2005) 582–586.
[37] S.W. Cao, Y.J. Zhu, J. Phys. Chem. C 112 (2008) 6253–6257.
[38] X.L. Zhang, C.H. Sui, J. Gong, Z.M. Su, L.Y. Qu, J. Phys. Chem. C 111 (2007) 9049–9054.
[39] A. Kaushik, R. Khan, P.R. Solanki, P. Pandey, J. Alam, S. Ahmad, B.D. Malhotra, Biosen. Bioelectron. 24 (2008) 676–683.
[40] S. Trévin, F. Bedioui, J. Devynck, J. Electroanal. Chem. 408 (1996) 261–265.
[41] W. Gerrard, Gas Solubilities: Widespread Applications, Pergamon, Oxford, 1980.
[42] X.H. Wang, L. Zhang, Y.H. Ni, J.M. Hong, X.F. Cao, J. Phys. Chem. C 113 (2009) 7003–7008.
[43] K.J. Mckenzie, F. Marken, Pure Appl. Chem. 73 (2001) 1885–1894.
[44] F. Marken, D. Patel, C.E. Madden, R.C. Millward, S. Fletcher, New J. Chem. 26 (2002) 259–263.